Microelectronics embedded in live jellyfish enhance propulsion

14 February 2020, by Thamarasee Jeewandara

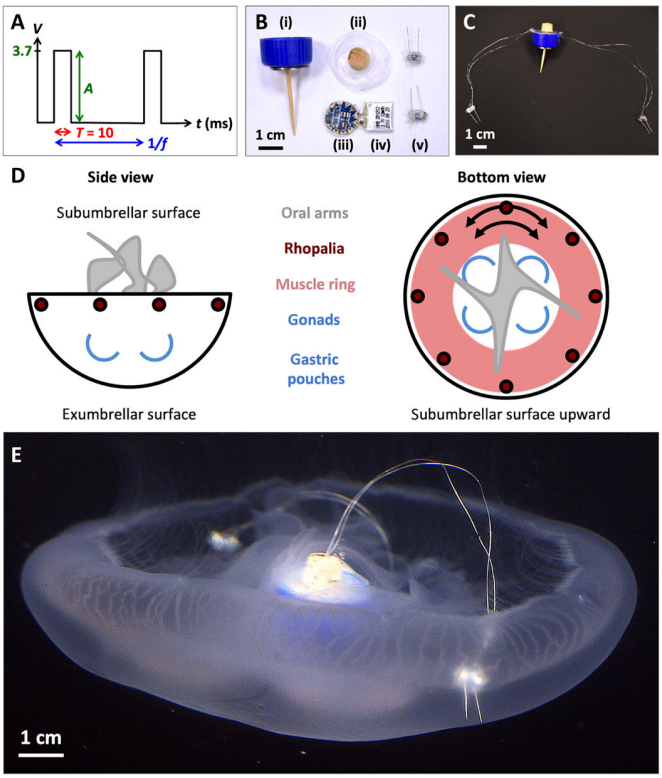

A. aurita swim controller design. (A) Square wave signal generated by the swim controller with an amplitude (A) of 3.7 V and a pulse width (T) of 10 ms, set at frequencies (f) of 0.25, 0.38, 0.50, 0.62, 0.75, 0.88, and 1.00 Hz. (B) Swim controller components. Housing includes (i) a polypropylene cap with a wooden pin that embeds into the bell center, and (ii) a plastic film to waterproof the housing, both offset with stainless steel and cork weights to keep the device approximately neutrally buoyant. Microelectronics include (iii) a TinyLily mini-processor, (iv) lithium polymer battery, and (v) two platinum-tip electrodes with LEDs to visually indicate stimulation. (C) Fully assembled device, with the processor and battery encased in the housing. (D) Simplified schematics of A. aurita anatomy, highlighting the subumbrellar (top) and exumbrellar (bottom) surfaces, rhopalia, muscle ring, and circumferential muscle fiber orientation, oral arms, and gonads/gastric pouches. (E) Swim controller (inactive) embedded into a free-swimming jellyfish, bell oriented subumbrellar side up, with the wooden pin inserted into the manubrium and two electrodes embedded into the muscle and mesogleal tissue near the bell margin. Photo credits for (B), (C), and (E): Nicole W. Xu, Stanford University. Credit: Science Advances, doi: 10.1126/sciadv.aaz3194

Researchers in robotic materials aim to artificially control animal locomotion to address the existing challenges to actuation, control and power requirements in soft robotics. In a new report in *Science Advances*, Nicole W. Xu and John O. Dabiri at the departments of bioengineering, civil and environmental engineering and mechanical engineering at the Stanford University presented a biohybrid robot that used onboard microelectronics to induce swimming in live jellyfish. They measured the ability to substantially enhance propulsion by driving body contractions at an optimal frequency range faster than natural behavior. The manoeuvre increased swimming speed by nearly threefold, although with only a twofold increase in metabolic expenditure of the animal and 10 mW of external power input to the microelectronics. The biohybrid robot used 10 to 1000 times less external power per mass than with previously reported aquatic robots. The capability can improve the performance scope of biohybrid robots relative to native performance, with potential applications as biohybrid ocean monitoring robots.

Jellyfish are a compelling model organism to form energy-efficient underwater vehicles due to their low cost of transport (COT). Existing biomimetic robots of swimming animals that are entirely built of engineered materials can achieve velocities comparable to natural animals, but with orders of magnitude less efficient than jellyfish. Biohybrid jellyfish robots can therefore integrate live animals to address existing challenges of soft robotics. Researchers can use the jellyfish structure for actuation and solve power requirements by exploring natural feeding behaviors where they extract chemical energy from prey in situ. The approach can also allow recovery from damage via

natural wound healing processes inherent to the animal, control animal locomotion and allow additional studies of live organism biomechanics in user-controlled experiments. In this study, Xu and Dabiri used a system of microelectronics to externally control a live jellyfish and form a biohybrid robot to advance science and engineering of aquatic locomotion.

In order to activate jellyfish as a natural scaffold, the team used the animal's own basal metabolism to reduce additional power requirements and leveraged its muscles for actuation while relying on self-healing and tissue regenerative properties for increased damage tolerance. The team hypothesized that increasing bell contraction frequencies of jellyfish could increase swimming speeds up to a limit. They therefore externally controlled the frequency of pulses in free-swimming animals by measuring the swim speed and oxygen intake to calculate the cost of transport (COT) and test their working hypothesis. Previously such examinations were only possible through computational or theoretical models.

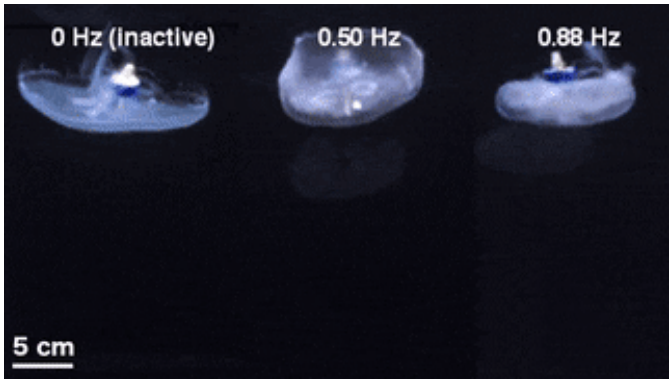

A comparison of bell geometries for unstimulated swimming with an inactive swim controller embedded (left) and externally controlled swimming at 0.50 Hz (middle) and 0.88 Hz (right). Credit: Science Advances, doi: 10.1126/sciadv.aaz3194

Xu et al. selected Aurelia aurita as a model organism; an oblate species of jellyfish containing a flexible mesogleal bell and monolayer of coronal and radial muscles lining the subumbrellar surface.

In order to swim, the organisms contracted muscles to decrease the subumbrellar cavity volume and eject water to provide a motive force alongside additional contributions from passive energy recapture and suction-based propulsion. To initiate these muscle contractions, the jellyfish activated any of its light pacemakers located in the sensor organs known as rhopalia along the bell margin. These nerve clusters activated the entire motor nerve net to cause bidirectional muscle wave propagations that originated from the activated pacemakers during natural propagation.

Robotic design integration in live jellyfish and device validation

The scientists first engineered a portable, self-contained microelectronic swim controller to generate a square pulse wave and stimulate muscle contractions from 0.25 Hz to 1.00 Hz. They composed the controller with a TinyLily mini-processor and a 10-mAh lithium polymer cell. To visually confirm the electrical signal, Xu et al. connected the wires in series to TinyLily light-emitting diodes (LEDs). They then inserted electrodes bilaterally into the subumbrellar tissue and kept the system naturally buoyant with stainless steel washers and cork. To validate that the swim controller could externally control jellyfish bell contractions, the scientists developed a method to track motion of the bell margin. For this, they completed three sets of experiments, (1) to observe endogenous contractions of the organism in the absence of any disturbances, (2) to observe if mechanically embedding inactive electrodes affected natural animal behavior and (3) to test stimulation protocols to confirm externally driven contractions.

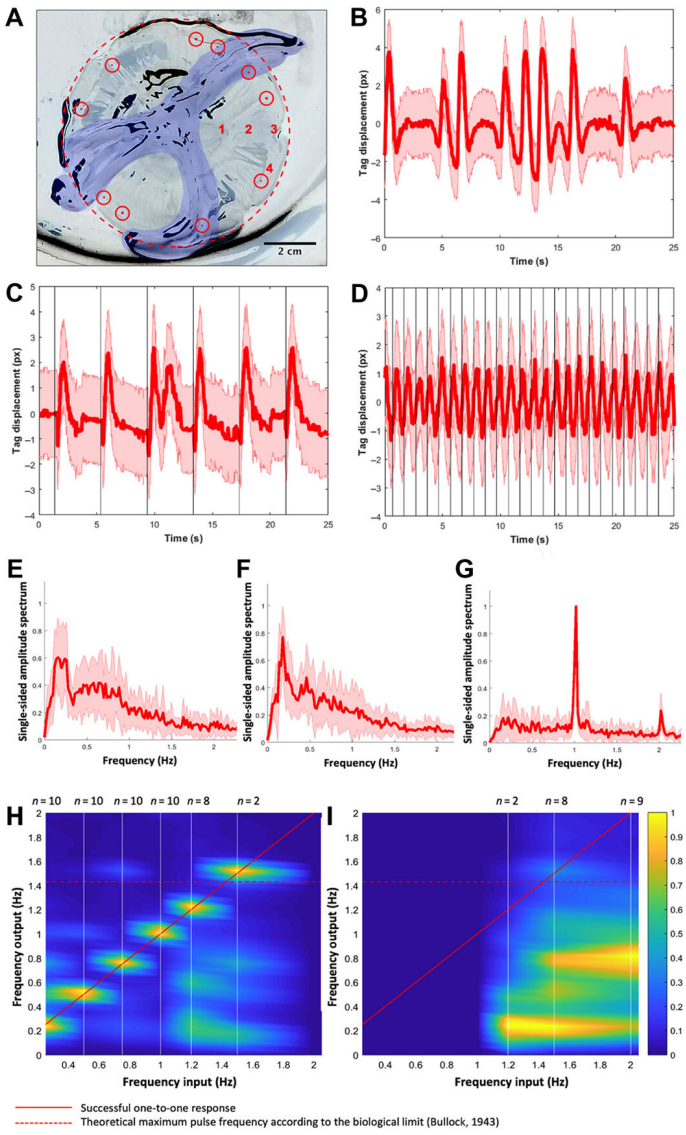

Signal validation using visual tags and frequency spectra to track muscle contractions. (A) A. aurita medusae (n = 10, 8.0 to 10.0 cm in diameter) were placed subumbrellar surface up in a plate without seawater for constrained muscle stimulation experiments (electrode not shown). The image is inverted so that the bell and plate are white, and black areas are reflections of light from animal tissue and the plate. For clarity, the margin of the bell is outlined in a red dotted circle, and the oral arms are colorized in blue. Visible implant elastomer tags (shown as colored red dots within red circles) were injected around the margin, and one tag was tracked per video to calculate the tissue displacement as a surrogate for muscle contractions. Spatial tests to determine whether electrode location affected the spectra were conducted at four locations, labeled in red numbers: (1) adjacent to the gastric pouches, (2) midway between the gastric pouches and margin, (3) at the rhopalia, and (4) at the margin away from the rhopalia. All other tests were conducted at location 2. (B) Example tag displacement as a function of time for an animal without any external stimulus. The red line indicates the centroid displacement, with the error calculated from assuming a half-pixel uncertainty in finding the centroid of the tag in each image, over 25 s. Note the temporal variation of muscle contractions, including periods of regular pulses and successive rapid pulses. (C) Example tag displacement for an animal with an external stimulus of 0.25 Hz, with each stimulus visualized as a vertical black line. Although contractions regularly follow external stimuli, natural animal pulses also occur at low frequencies. Note, for example, the double pulse after one stimulus (t ? 12 s). (D) Example tag displacement for an animal with an external stimulus of 1.00 Hz, with each stimulus visualized as a vertical black line. The same time window (25 s) is shown for a fair comparison to the previous two plots. Contractions regularly follow external stimuli. (E) single-sided amplitude spectrum (SSASs) averaged for jellyfish without any external stimulus (n = 12 for 10 animals, i.e., 2 jellyfish had two replicate clips each). The red line indicates the mean of normalized SSAS for each replicate, with the SD in pink. The peak of the mean SSAS is at 0.16 Hz. The full width at half maximum (FWHM) is 0.24 Hz. (F) Jellyfish response to an inactive electrode embedded (n = 14 for 10 animals, i.e., 4 jellyfish had two replicate clips each). The peak of the mean SSAS is at 0.18 Hz. The FWHM is 0.16 Hz. Using a two-sample t test of the peak frequencies for both groups, the difference between the two samples was statistically insignificant (P = 0.68). (G) Sample SSAS for an electrical stimulus at 1.00 Hz (n = 10 jellyfish for an input signal of 4.2 V and 4.0 ms). The peak frequency occurs at 1.02 Hz, within the 0.02 window used to calculate the SSAS. Note that the spectrum has a sharper peak at the frequency of interest (FWHM of 0.04 Hz), as opposed to a wider FWHM in (B) and (C), the cases without any external stimulus. (H) Contour map of the frequency response of muscle contractions to external electrical stimuli. Each vertical line of data (centered on white lines at 0.25, 0.50, 0.75, 1.00, 1.20, 1.50, and 2.00 Hz) represents the PSD at one electrical input frequency, with the number of jellyfish tested shown above. The colors correspond to the amplitude of the PSD, in which higher values are shown in yellow and lower values in blue. The solid red line represents a one-to-one input-output response, and the dashed red line represents the reported physiological limit according to the minimum absolute refractory period of A. aurita muscle (32). Responsive trials are defined by whether the peak frequencies in the PSD lie within a window of 0.06 Hz of the solid red curve. (I) Contour maps of the unresponsive trials. Higher frequencies up to 90.00 Hz were also tested with similar unresponsive PSDs. Photo credit for (A): Nicole W. Xu, Stanford University. Credit: Science Advances, doi: 10.1126/sciadv.aaz3194

They found that natural animal behavior (or endogenous contraction) was irregular with high pulse rate variability—including a mean peak frequency of 0.16 Hz. An inactive electrode did not significantly change the frequency spectra, while externally driven contractions showed a physiological limit of jellyfish muscle contractions between 1.4 Hz to 1.5 Hz. The team conducted swimming trials with the implanted system in a saltwater tank and normalized the measured swimming speeds to account for variation in animal size. They scaled the normalized swimming speed by the mean of the normalized speed in the absence of stimulation (i.e. 0 Hz) to determine the enhancement factor. The maximum enhancement factor was up to 2.8 times the natural swimming speed of the animals, i.e., the swimming speed enhanced up to 2.8 times using onboard microelectronics.

Highly efficient device power consumption

The artificially controlled jellyfish required external power from the microelectronic system and internal power from the animals' own metabolism. When driven at increasing frequencies, the microelectronic system of the biohybrid robotic jellyfish consumed greater Watts per kg. However, compared to existing robots, this biohybrid robot used up to 1000 times less external power. Xu et al. compared this prototype with the medusoid and robotic ray made from rat cardiomyocytes seeded on silicon scaffolds, and with purely mechanical robots as well as autonomous underwater vehicles (AUVs). In addition to the cost-effective benefits of low external power consumption per mass of the biohybrid robot, the microelectronic system only cost less than $20 from commercially available components. The electrolocation was also non-specific and the animals immediately recovered after the experiments.

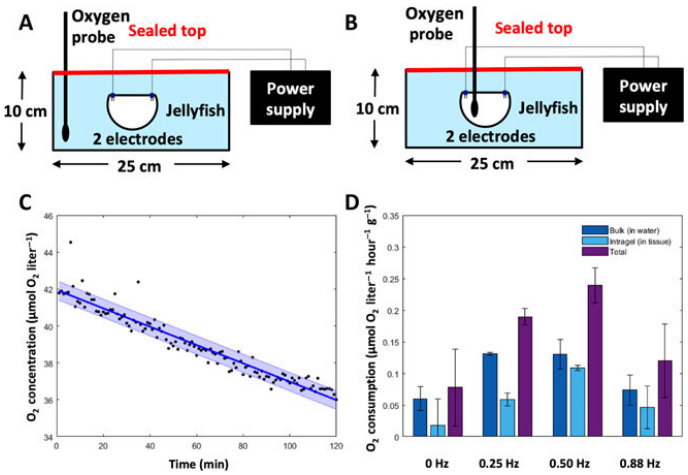

Metabolic rate experiments. To determine the metabolic rate of jellyfish, oxygen concentrations were measured in animal tissue and the surrounding water and then converted into energy expenditure. (A) Experimental setup to measure bulk dissolved oxygen concentrations (in the water). Animals were placed subumbrellar surface upward in a sealed glass dish filled with 2 liters of artificial seawater, with two electrodes for frequency-driven cases. Oxygen levels in the water were measured using a MicroOptode oxygen probe. (B) Experimental setup to measure intragel oxygen concentrations (in the tissue). Animals were placed subumbrellar surface upward in a sealed glass dish filled with 2 liters of artificial seawater, with two electrodes for frequency-driven cases. Intragel oxygen levels were measured using a MicroOptode oxygen probe embedded into the tissue. (C) Representative plot of oxygen concentrations over time, measured from the MicroOptode. This example shows measurements of bulk oxygen levels in the water surrounding an animal with a swim controller–driven frequency of 1.00 Hz. Individual data points are shown in black, the best-fit line is shown in dark blue, and the SD is shown in the light blue shaded region. (D) Oxygen consumption rates of the surrounding water (dark blue), within animal tissue (light blue), and total (sum of the water and tissue measurements, purple) were calculated over a 6- to 8-hour period (n = 7 animals).Credit: Science Advances, doi: 10.1126/sciadv.aaz3194

The new capability of external control allowed Xu et al. to address the relationship between swimming frequency and metabolic rate. Oxygen consumption rates followed a similar pattern to enhanced swimming speeds, and the scientists calculated the equivalent cost of transport using both experimental

metabolic rates and experimental swimming speeds. The COT increased at mid-range frequencies and decreased at high external stimulation frequencies. The results showed that enhanced jellyfish swimming did not cause undue cost to the metabolism or health of the animal.

The main robotic limit of the study was the power requirement of the microelectronic system relative to animal versus microelectronic power needs. Further improvement to microelectronics can decrease the energetic costs and extended studies can also strive to minimize endogenous animal contractions without harming the organism to improve controllability of live-animal-based biohybrid robots. The artificial control of jellyfish can expand ocean monitoring techniques with improved controllability by incorporating microelectronic sensors to leverage the existing tagging technology .

More information: Nicole W. Xu et al. Low-power microelectronics embedded in live jellyfish enhance propulsion, *Science Advances* (2020). DOI: 10.1126/sciadv.aaz3194

XI. The Croonian lecture.—Preliminary observations on the locomotor system of medusæ, Published:01 January 1876. *Philosophical Transactions*. doi.org/10.1098/rstl.1876.0011

Guang-Zhong Yang et al. The grand challenges of Science Robotics, *Science Robotics* (2018). DOI: 10.1126/scirobotics.aar7650

APA citation: Microelectronics embedded in live jellyfish enhance propulsion (2020, February 14) retrieved 28 September 2020 from https://techxplore.com/news/2020-02-microelectronics-embedded-jellyfish-propulsion.html